ACS APPLIED MATERIALS & INTERFACES

Research Article

www.acsami.org

Bismuth-Doped Tin Oxide-Coated Carbon Nanotube Network: Improved Anode Stability and Efficiency for Flow-Through Organic Electrooxidation

Han Liu, Akshay Vajpayee, and Chad D. Vecitis*

School of Engineering and Applied Sciences, Harvard University, Cambridge, Massachusetts 02138, United States

Supporting Information

ABSTRACT: In this study, a binder-free, porous, and conductive 3D carbon-nanotube (CNT) network uniformly coated with bismuth-doped tin oxide (BTO) nanoparticles was prepared via a simple electrosorption−hydrothermal method and utilized for the electrooxidative filtration of organics. The BTO-CNT nanocomposite was characterized by scanning electron microscopy, thermogravimetric analysis, transmission electron microscopy, X-ray photoelectron spectroscopy, linear sweep voltammetry, and Tafel analysis. The submonolayer BTO coating is composed of 3.9 ± 1.5 nm diameter nanoparticles (NPs). The oxygen-evolution potential of the BTO-CNT nanocomposite was determined to be 1.71 V (vs Ag/AgCl), which is 440 mV higher than an uncoated CNT anode. Anodic stability, characterized by CNT oxidative corrosion to form dissolved species, indicated that the BTO-CNT incurred negligible corrosion up to V_{anode} = 2.2 V, whereas the uncoated CNT was compromised at $V_{anode} \geq 1.4$ V. The effect of metal oxide-nanoparticle coating on anodic performance was initially studied by oxalate oxidation followed by total organic carbon (TOC) and chemical oxygen demand (COD) analysis. The BTO-CNT displayed the best performance, with ∼98% oxalate oxidation (1.2 s filter residence time) and current efficiencies in the range of 32 to >99%. The BTO-CNT anode energy consumption was 25.7 kW h $kgCOD^{-1}$ at ∼93% TOC removal and 8.6 kW h $kgCOD^{-1}$ at ∼50% TOC removal, comparable to state-of-the-art oxalate oxidation processes (22.5−81.7 kW h $kgCOD^{-1}$). The improved reactivity, current efficiency, and energy consumption are attributed to the increased conductivity, oxygen-evolution potential, and stability of the BTO-CNT anode. The effectiveness and efficiency of the BTO-CNT anode as compared to the uncoated CNT was further investigated by the electrooxidative filtration of ethanol, methanol, formaldehyde, and formate, and it was determined to have TOC removals 2 to 8 times greater, mineralization current efficiencies 1.5 to 3.5 times greater, and energy consumption 4 to 5 times less than the uncoated CNT anode. Electrooxidation and anode passivation mechanisms are discussed.

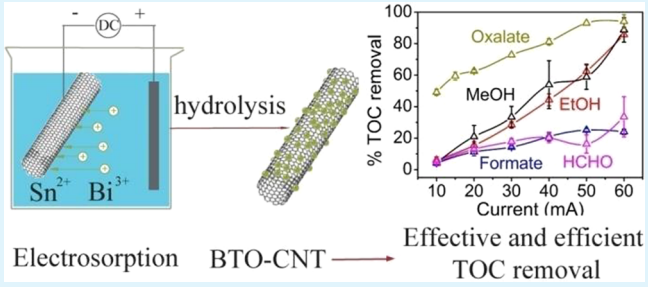

KEYWORDS: *carbon nanotubes (CNT), filter, bismuth-doped tin oxide, anode stability, current efficiency, organic oxidation*

INTRODUCTION

Carbon nanotubes (CNTs) are widely used in electrochemical applications including batteries,[1,2] super-capacitors,[3,4] and fuel cells[5,6] because of their unique physical and chemical properties. One promising general electrochemical application of CNTs is anodic organic oxidation, which is relevant to water treatment, fuel cells, and sensors. Because of their high aspect ratio, large specific surface area, excellent conductivity, and stable chemical structure, CNTs can potentially form porous, conductive, and 3D structures for effective, efficient, and rapid electrochemical oxidation.[7,8]

For example, recent studies have shown that a porous CNT electrochemical filter, where the solution to be treated flows though the electrode, can effectively remove organic dyes, phenol, and ions via adsorption and electrooxidation.[7] The flow-through filter configuration results in electrochemical kinetics up to 10 times greater as compared to the conventional batch electrochemical reactor configuration because of increases in the convective mass transfer of the target molecules to the electrode surface.[9,10] Nevertheless, the electrochemical filter CNT anode still faces the same universal anode development challenge: low current efficiencies at high anode potentials as a result of competition with anode corrosion and water oxidation (eq 1).[9,11]

$$2H_2O \rightarrow O_2 + 4e^- + 4H^+ \quad (E^\circ = 1.03\ \text{V vs Ag/AgCl}) \tag{1}$$

The oxygen-evolution reaction will substantially reduce the current efficiency (CE) because the solvent water (55 M) will always be in great excess relative to the target molecules, limiting electrochemical oxidation applications at anode potentials over their oxygen evolution overpotential (OEP).

Received: July 2, 2013
Accepted: September 16, 2013
Published: September 16, 2013

For example, the electrochemical oxidation of recalcitrant perfluorinated molecules such as perfluorooctanoate (PFOA) required anode (Ti/SnO_2-Sb-Bi) potentials >3.4 V for rapid oxidation, resulting in a current efficiency of less than 1%.[12]

A low OEP may be problematic for uncoated CNT anodes. For example, a CNT OEP of ~1.0 V (vs Ag/AgCl) has been reported, indicating a negligible oxygen-evolution overpotential and resulting in significant decreases (~70%) in dye oxidation current efficiency at ~200 mV > OEP.[9] In addition, a recent study on the durability of single-wall carbon nanotubes indicated that high anode potentials (>4 V) caused severe CNT degradation in deionized water,[13] which would significantly deteriorate anode conductivity and performance. Therefore, the development of novel anode materials with increased OEP (and in turn target-molecule current efficiency) as well as stability is of great importance, in particular for organic oxidation processes requiring high anode potentials.

Fortunately, CNTs are not only effective as a homogeneous anode material but can also serve as an excellent high surface area catalyst substrate. Surface modification with selected organic,[20] inorganic,[21,22] and biological species[23,24] dramatically influences the CNT chemical and physical properties and can improve device performance for many electrochemical applications such as fuel cells,[14,15] super-capacitors,[3,16] and Li-ion batteries.[17−19] For example, a range of inorganic nanoparticle (NP)-CNT composites such as Fe_3O_4-CNT,[25] MnO_2-CNT,[26] and SnO_2-CNT (TO-CNT)[27] have been synthesized by reactive sputtering or hydrothermal methods and evaluated for Li-ion battery applications. In regards to electrochemical organic oxidation applications, SnO_2 and doped-SnO_2 are common inorganic anode-coating materials because SnO_2 has one of the highest reported OEPs at 1.7 V versus Ag/AgCl.[28] For example, a TiO_2 nanotube (TiO_2-NT) loaded with Sb-doped SnO_2 (ATO) NPs of 20 nm in diameter demonstrated an OEP of 1.6 V versus Ag/AgCl and was effective for the mineralization of benzoic acid:[29]

$$C_6H_5COOH + 12H_2O \rightarrow 7CO_2 + 30H^+ + 30e^- \quad (2)$$

The mineralization current efficiency (MCE) was greatly improved from 0.4% for the TiO_2-NT anode to 14.2% for the ATO coated TiO_2-NT anode. Therefore, one strategy to improve the current efficiency of high-potential CNT anode applications may be to coat a thin layer of high-OEP-doped tin oxide nanoparticles onto the CNT network.

Although a significant number of interesting works have been published on the coating of tin oxide or doped tin oxide nanoparticles (NPs) onto a carbon-nanotube substrate, we could not find any reported material synthesis method that met all of the requirements for a CNT anode operating in the flow-through configuration. Because of the nature of high-potential Faradaic electrochemical filtration, three key challenges in CNT-metal oxide anode preparation must be addressed: (I) a binder-free conductive CNT network, (II) a mechanically stable 3D porous structure viable for fluid filtration, and (III) a high-OEP CNT-metal oxide nanocomposite with minimal toxicity. First, many hydrothermal or sol-gel methods for SnO_2-coated CNT synthesis[30,27,31] depend on conductive additives, such as carbon black and polymer binders, to lower the electrical resistance and increase mechanical stability. However, additives may result in competitive oxidation and block reactive sites,[32] so binder-free and conductive CNT-metal oxide network materials are of great interest (key challenge I). Second, although there are few studies that successfully developed binder free and conducting SnO_2-CNT networks,[32] a thin layer of CNTs must first be deposited on a metal substrate such that the NP coating can be formed via chemical vapor deposition. The final product is a network attached to the metal substrate that cannot be used as a flow-through electrode (key challenge II). Third, tin oxide is a semiconductor with a large band gap of 3.5 eV and is typically doped with Sb (toxic substance with an EPA drinking water limit of 6 $\mu g\ L^{-1}$)[33] to increase the conductivity and electrochemical oxidation kinetics (key challenge III).[28,34,35] Therefore, it is of interest to develop a highly conductive, stable, binder-free, non-toxic, and porous 3D CNT network to improve the anodic performance of high-potential, flow-through, organic oxidation applications.

In this study, we have prepared a porous CNT network coated with Bi-doped tin oxide (BTO) NPs and investigated its potential to overcome the three key challenges discussed above. Initial experiments compared the anodic performance of the uncoated CNT, tin oxide-coated CNT (TO-CNT), antimony-doped tin oxide-coated CNT (ATO-CNT), and bismuth-doped tin oxide-coated CNT (BTO-CNT) to determine if Bi was an effective and non-toxic alternative to Sb by measuring OEP, Tafel slope, and organic mineralization current efficiency. The composite is prepared using the electrosorption of metal ions at the desired mole ratio onto a preformed 3D porous CNT network to ensure CNT−CNT contact followed by thermal hydrolysis at 80 °C for 1 h in pure water to precipitate the metal oxide coating. After hydrolysis, the metal oxide-CNT composite anode can be immediately used for electrochemical filtration. The metal oxide-CNT anodes were characterized by scanning electron microscopy (SEM), transmission electron microscopy (TEM), X-ray photoelectron spectroscopy (XPS), and thermogravimetric analysis (TGA). The oxygen evolution of the metal oxide-CNT composites was examined by linear sweep voltammetry (LSV) and Tafel analysis. The anodic performance of the composite materials were examined by challenging with 1 mM oxalate, a recalcitrant organic.[36] Once enough evidence was collected demonstrating that the non-toxic BTO-CNT anode was as effective and efficient as the ATO-CNT anode, further experiments were completed only with the uncoated CNT control and BTO-CNT anodes. A stability test of the uncoated CNT and BTO-CNT anodes was completed by challenging the anode with only electrolyte or no electrolyte and measuring the effluent total carbon (TC) and inorganic carbon (IC), which are indicators of CNT electro-oxidative corrosion. The anode materials before and after the stability test were also analyzed by XPS. Finally, the CNT and BTO-CNT anodic performance towards a range of small organics was evaluated. Electrooxidation and anode passivation mechanisms are discussed.

MATERIALS AND METHODS

Chemicals and Materials. Sodium sulfate (Na_2SO_4, ≥98.0%), sodium persulfate ($Na_2S_2O_8$, ≥98.0%), tin chloride dihydrate ($SnCl_2 \cdot 2H_2O$, ≥98.0%), antimony chloride ($SbCl_3$, ≥99.0%), bismuth nitrate pentahydrate ($Bi(NO_3)_3 \cdot 5H_2O$, ≥98.0%), hydrochloric acid (HCl, 36.5-38.0%), phosphoric acid (H_3PO_4, 85%), sodium oxalate ($Na_2C_2O_4$, ≥99.5%), ethanol (EtOH, ≥99.5%), methanol (MeOH, 99.8%), formaldehyde (HCHO, 36.5−38% in H_2O), and sodium formate (HCOONa, ≥99.0%) were purchased from Sigma-Aldrich (St. Louis, MO). All chemicals were reagent grade. All aqueous solutions were made with water from a Barnstead Nanopure Infinity purification system that produced water with a minimal resistivity of 18 $M\Omega\ cm^{-1}$. The multiwalled carbon-nanotubes networks were purchased from NanoTechLabs (Buckeye Composites, Yadkinville,

NC) in circles that were 47 mm in diameter, 41 ± 8 μm in depth, ~85% pore volume, and had an average pore size of 104 ± 39 nm, as have been characterized previously in detail.[10]

Electrooxidative Filter Preparation. The NP-CNT nanocomposite anode was prepared via a simple electrosorption–hydrothermal method. To prepare the TO-CNT, 1 g of $SnCl_2{\cdot}2H_2O$ was dissolved in 33 mL of 37% HCl followed by the addition of 67 mL of deionized water. The solution was bath sonicated for 15 min and used as the electrolyte for electrosorption. The CNT network (40 mg) was first wetted with ethanol prior to electrosorption. The electrosorption process utilized a conventional bipolar electrochemical cell that was placed into the electrolyte solution using the CNT network as the cathode and a titanium plate (3 × 2 cm^2) as the anode. The total applied voltage was 1 V for 1 h. During the electrosorption process, the CNT cathode becomes negatively charged and in turn electrosorbs the positively charged metal cations. After electrosorption, the CNT network was placed in a hot (80 °C) DI water bath for 1 h to precipitate the metal oxides. The coated CNT filter was then removed from the hot water bath and dried in air at 60 °C for 2 h. The ATO-CNT and BTO-CNT preparation processes were exactly the same as that of the TO-CNT except that 0.050 g $SbCl_3$ or 0.107 g $Bi(NO_3)_3{\cdot}5H_2O$ was also added to the electrolyte solution such that the molar ratio of dopant (Sb or Bi) to Sn was 0.05. The anodic filter was then loaded into a filtration casing modified for electrochemistry, as described in detail in a previous study[7] (Figure S1).

SEM. SEM was completed in Harvard's Center for Nanoscale Systems (CNS) on a Zeiss FESEM Ultra Plus. Micrographs were analyzed with ImageJ (NIH) software to determine CNT diameter and aerial pore diameter, which is the distance between CNTs. Reported diameters were the average of at least 100 measurements from at least two network images.

TEM. TEM was completed at Harvard's Center for Nanoscale Systems on a JEOL 2100TEM with an accelerating voltage of 200 kV. Prior to imaging, BTO-CNT powder was scratched from the BTO-CNT filter and spread onto a copper grid for analysis. Nanoparticle size measurements were the average of at least 100 measurements from at least two network images.

XPS. XPS was completed on a Thermo Scientific K-Alpha XPS with a monochromatic Al Kα X-ray source in Harvard's Center for Nanoscale Systems. Survey spectra were scanned for all samples from 0 to 1400 eV to determine the elemental composition near the CNT network surface. Individual element scans were also completed for C 1s (274–294 eV), O 1s (522–542 eV), Sn 3d (477-500 eV), and Bi 4f (154-169 eV). Avantage software was used to determine the integrated peak areas for the individual elements and to estimate the surficial carbon-nanotube network elemental ratios.

TGA. TGA was completed in Harvard's Material Research Science and Engineering Center (MRSEC) on a Q5000-IR Thermogravimetric Analyzer (TA Instruments). Samples were ground into powder and placed in a platinum pan. The initial sample weight was ~5.2 mg for the uncoated CNT network and ~6.4 mg for the BTO-CNT network. The pan was heated from room temperature to 150 °C at 10 °C min^{-1}, held at 150 °C for 30 min to remove any residual water, heated to 800 °C at 10 °C min^{-1}, held at 800 °C for 30 min, and was finally brought back to room temperature at 20 °C min^{-1}. A second identical run was completed immediately after the first and used as a background. The percent of residual material was determined using the initial mass and the mass remaining after a complete thermal cycle.

Electrochemical Characterization. The LSV and Tafel experiments were completed with a CHI604D electrochemical workstation (CH Instruments, Inc.) utilizing a Ag/AgCl reference electrode, a perforated titanium shim counter electrode, and an uncoated CNT or a metal oxide coated CNT network as the working electrode in the conventional batch (no flow) configuration. The electrochemical cell was placed into 500 mL of 0.5 M H_2SO_4 for LSV and Tafel analysis. Scan rates of 0.02 and 0.01 V s^{-1} were used for LSV and Tafel analysis, respectively. The anode used for electrochemical characterization had an active geometric area of 7 cm^2 and a mass of 16 mg CNT plus metal oxide. The total surface area was obtained by multiplying the CNT mass by its BET specific surface area, 88.5 m^2 g^{-1},[7] which in this case was 1.4 m^2.

Electrooxidative Filtration. A background electrolyte of 10 mM sodium sulfate in water was used for all experiments unless otherwise noted. Oxalate, ethanol, methanol, formaldehyde, and formate at different concentrations were used as target molecules for electrooxidative filtration. Although the uncoated or coated CNT networks were circles of 47 mm in diameter, only an inner circle with a diameter of 30 mm was in contact with solution, with the rest buried by the rubber seal. Thus, in all experiments, the effective anodic filter was composed of 16 mg of CNT and any additional NPs. The exposed geometric area was 7 cm^2, and the total surface area was 1.4 m^2. The flow rate (J) in the oxalate experiments was 1.5 mL min^{-1} and for all other electrooxidative filtration experiments was 3 mL min^{-1}. The thickness of the CNT filter was 45 μm, so the residence time was ~1.2 s for oxalate experiments and ~0.6 s for all other electrooxidative filtration experiments. The electrooxidative filtration was completed at a number of controlled currents ranging from 1 to 60 mA. The controlled-current method was used here such that the current efficiency can be easily calculated and compared to previous organic electrooxidation studies that utilize constant-current methods. The steady-state effluent total organic carbon (TOC) was measured after the current was constant for 20 minutes, and the mineralization current efficiency (MCE) was calculated by the following equation

$$\mathrm{MCE} = \frac{(\mathrm{TOC}_{\mathrm{inf}} - \mathrm{TOC}_{\mathrm{eff}})n_e F J}{12 I} \quad (3)$$

where TOC_{inf} and TOC_{eff} stand for the influent and effluent TOC in mg L^{-1}, n_e is the average number of electrons transferred per carbon to oxidize to carbon dioxide, F = 96 485 C mol^{-1} is Faraday's constant, J is the flow rate in L s^{-1}, and I is the current in mA. The time-averaged voltage at each current was also recorded and used to calculate the energy consumption (EC) in kW h $kgTOC^{-1}$ by the following equation

$$\mathrm{EC} = \frac{UI}{3600(\mathrm{TOC}_{\mathrm{inf}} - \mathrm{TOC}_{\mathrm{eff}})J} \quad (4)$$

where U and I denote the measured voltage (V) and current (mA).

Anode Stability Test. The anode stability tests of the uncoated CNT and BTO-CNT networks were completed with a CHI604D electrochemical workstation using an Ag/AgCl reference electrode, a perforated titanium shim counter electrode, and an uncoated CNT or metal oxide coated CNT network as the working electrode. For the stability experiments, either DI water or 10 mM electrolyte (Na_2SO_4 or NaF) was flowed through the working electrode at a set anode potential and a flow rate of 1.5 mL min^{-1}. The anode potential was increased stepwise from 0.6 to 3.0 V and kept at each potential for a time interval of 10 min. The time dependence of the effluent concentration for the CNT stability test was measured, and the results (Figure S2) indicate that a measurement at 10 min represents an extended time average. The steady-state current, TC, and IC measurements of the effluent were taken at the end of each interval.

TOC Measurement. The TOC analyses were completed on a Shimadzu TOC-VW analyzer equipped with a UV/thermal persulfate oxidizer. The calibration was completed over a concentration range of 1 to 100 mg C L^{-1} using a six-point curve with potassium terephtalate as a carbon source. The TC injection was 1.5 mL per sample with the addition of 75 μL of 0.5 M sodium persulfate and 75 μL of 17% phosphoric acid. The IC injection was 2.5 mL per sample with the addition of 125 μL of 17% phosphoric acid.

RESULTS AND DISCUSSION

Anode Material Characterization. The uncoated CNT and BTO-CNT networks were characterized by SEM and TEM for surface morphology, XPS for surface elemental composition analysis, and TGA for NP loading as well as electrochemical characterization for OEP and Tafel slopes. The surface morphology of the BTO-CNT nanocomposite prepared is of

interest because the size and uniformity of the NP coating may significantly alter the physical and chemical properties of the material and in turn its effectiveness.[37] An SEM image of the uncoated CNT network is displayed in Figure 1a. The CNTs

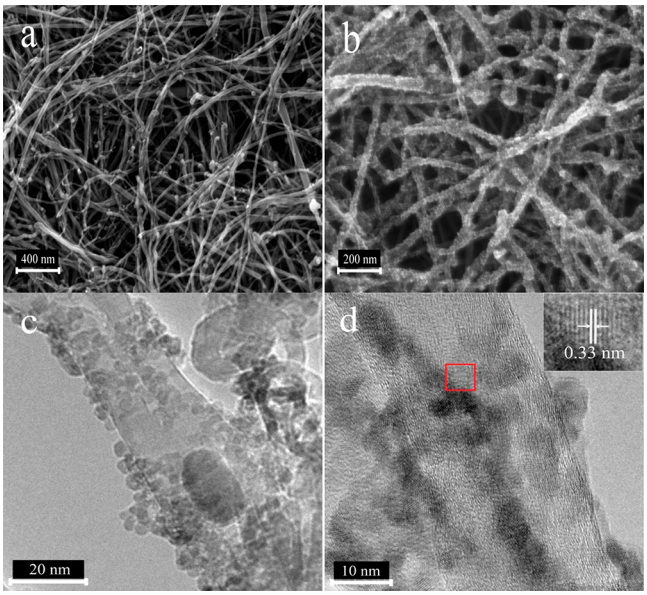

Figure 1. Electron microscopy images of representative anode networks. (a) Aerial SEM image of the uncoated CNT network. (b) Aerial SEM image of the BTO-CNT network. (c) TEM image of the BTO-CNT nanocomposite analyzed for NP size and coating thickness. (d) Magnified view of BTO crystals on the CNT surface with the inset showing the lattice spacing of a BTO particle in the red square.

have an average diameter of 19.6 ± 9.9 nm, exhibit a clean and smooth surface, are randomly oriented in a 2D plane, and form a porous and conductive 3D network viable for electrochemical filtration. An aerial SEM image of the CNT network after BTO NP deposition is displayed in Figure 1b. The CNT surfaces are uniformly coated by the BTO NPs as they become significantly rougher, and no bulk (>10 nm) tin oxide particles are observed.

TEM images of the BTO-CNT nanocomposite network are displayed in Figure 1c,d. The BTO coating on the CNT networks has a thickness of <10 nm and a uniform particle size of 3.9 ± 1.5 nm. There is also a large particle of ∼20 nm located inside one of the CNTs, which can be attributed to the residual Fe catalyst because similar particles were also observed inside the uncoated CNTs. A magnified view of a BTO NP (Figure 1d) at the surface of a CNT indicates that the NPs are crystalline with distinct lattice fringes. The adjacent spacing of aligned lattice fringes is 0.33 nm, slightly larger than the spacing of the (110) plane of a pure SnO_2 crystal, 0.32 nm, possibly due to the Bi doping because Bi has a slightly larger atomic radii (1.60 Å) than Sn (1.45 Å).[38] Together, the SEM and TEM images show that the uniformly coated BTO-CNT network prepared in this study is free-standing, binder-free, and porous and is thus suitable for electrochemical filtration (key challenges I and II).

The uncoated CNT and BTO-CNT networks were also characterized by XPS and TGA analysis. The surficial elemental compositions (XPS) are summarized in Table 1, and the XPS survey scans can be found in Figure S3. XPS indicates that the uncoated CNT surface elemental composition is 0.51% O, 0.14% Fe, and 99.35% C. The observed iron is attributed to the residual iron catalyst from the CNT synthesis.[7] For comparison, the BTO-CNT surface elemental composition is 11.6% O, 83.6% C, 4.7% Sn, and 0.1% Bi, and no surface iron was detected, possibly due to dissolution in the acidic (pH 2 to 3) electrosorption solution. From the surficial elemental composition, the Sn/C atomic ratio is 0.056. The nanocomposite Bi/Sn atomic ratio is 0.02, which is lower than the electrosorption solution Bi/Sn atomic ratio of 0.05. The mass of the nanoparticle coating was evaluated by TGA (Figure S4 and Table 1). The remaining mass of the uncoated CNT sample after combustion (800 °C) was 2.5% of its original weight and can be attributed to the residual Fe catalyst. This result is consistent with previous reports,[10] but it is much higher than the Fe content as determined by XPS analysis (0.14% atomic ratio or 0.65% weight), indicating that most of the residual catalyst is within tubes, in agreement with the large internal particles observed by TEM in Figure 1c. The BTO-CNT sample had a significantly greater residual mass of 17.4%, as expected because of the addition of the inorganic BTO NP coating. Assuming the same iron oxide/carbon weight ratio of the uncoated CNT sample holds in BTO-CNT, the actual weight ratio of BTO nanoparticles/carbon is determined to be 0.185. The TGA burn temperature of the BTO-CNT network is 630 °C, which is slightly (5 °C) higher than the burn temperature of the uncoated CNT, 625 °C, indicating negligible degradation of the CNT stability during the coating process. In summary, the BTO NP loading on the CNT network was 18.5% with regards to carbon weight, and the Bi doping was 2% with regards to Sn.

As previously discussed, the OEP is an important operational parameter for anode materials used in high-voltage applications such as organic oxidation.[39] The oxygen-evolution potential and kinetics of the four electrodes, uncoated CNT, TO-CNT, ATO-CNT, and BTO-CNT, were examined by both LSV and Tafel analysis. The linear sweep voltammograms (scan rate = 0.02 V s^{-1} in 0.5 M H_2SO_4 solution) for the four anode materials are presented in Figure 2a (solid lines). The subsequent extrapolations (dashed lines) of the current waves to 0 A was used to determine the oxygen-evolution potentials (vs Ag/AgCl) of the uncoated CNT (black, 1.27 V) < ATO-CNT (blue, 1.51 V) < BTO-CNT (pink, 1.71 V) < TO-CNT (red, 1.85 V) anodes. The OEP of TO-CNT is 150 mV higher than the reported OEP of bulk SnO_2, 1.7 vs Ag/AgCl,[28] which not only verifies that the NP deposition method used here leads

Table 1. Material Characterization by XPS and TGA

sample	C, %[a]	O, %[a]	Fe, %[a]	Na, %[a]	S, %[a]	Sn, %[a]	Bi, %[a]	res, %[b]	burn peak (°C)[b]
CNT	99.35	0.51	0.14					2.5	625
CNT 1.8 V	87.41	9.82	0.61	1.57	0.58				
BTO-CNT	83.62	11.56				4.72	0.10	17.4	630
BTO-CNT 3 V	70.26	17.92		5.78	1.77	4.18	0.08		

[a]Determined by XPS, atomic percentage. [b]Determined by TGA, weight percentage.

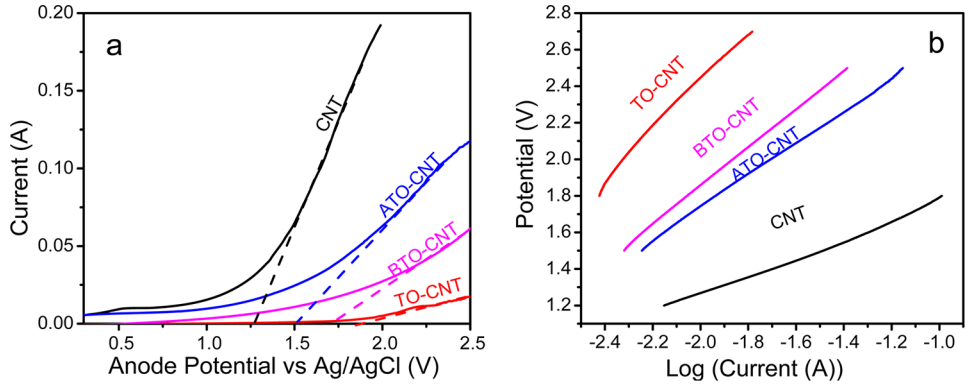

Figure 2. Electrochemical characterization of the anode materials. (a) Linear sweep voltametry (LSV). (b) Tafel plots. The LSV and Tafel experiments were completed with a scan rate of 0.02 and 0.01 V s^{-1}, respectively, in a 0.5 mol L^{-1} H_2SO_4 solution. The CNT voltammogram is given as the black solid line, ATO-CNT, blue, BTO-CNT, pink, and TO-CNT, red. The dashed lines are extrapolations to determine the OEP of each anode. The geometric area of the porous anode was 7 cm^2, and the total surface area of the porous anode was 1.4 m^2.

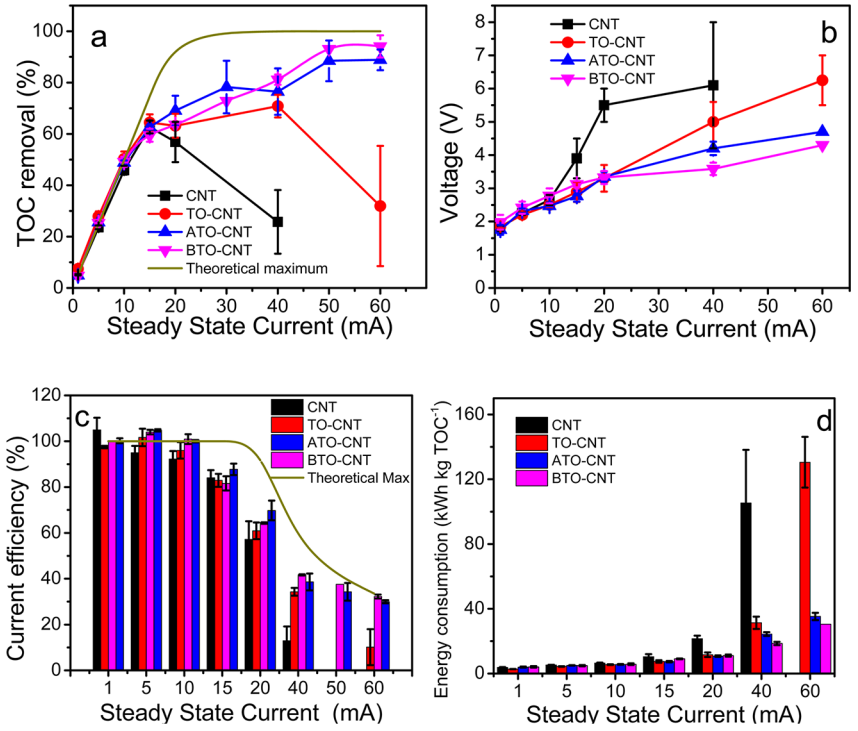

Figure 3. Electrochemical filtration of oxalate with the various anode materials as a function of steady-state current. (a) TOC removal (%). (b) Total cell voltage (V). (c) Current efficiency (%). (d) Energy consumption (kW h $kgTOC^{-1}$). The uncoated CNT results are in black, TO-CNT, red, ATO-CNT, blue, and BTO-CNT, pink. The dark-yellow line in panel c represents the theoretical maximum of current efficiency assuming 100% TOC removal. TOC_{inf} = 100 mg C L^{-1}, J = 1.5 mL min^{-1}, residence time 1.2 s, and $[Na_2SO_4]$ = 10 mM.

to an effective and uniform coating on the CNT surface but also indicates that the SnO_2 NPs may have a higher OEP than bulk SnO_2. As the particle size decreases to the nanoscale (<10 nm), the band gap will increase because of quantum confinement as compared to the bulk material and may in turn affect the material OEP by lowering the valence band edge. For example, SnO_2 NPs with a diameter of 3−5 nm were reported to have band gap of 4.05 eV, which is 0.35 eV larger than that of the bulk SnO_2 band gap of 3.7 eV.[40] The OEP (vs Ag/AgCl) of the TO-CNT (1.85 V) and BTO-CNT (1.71 V) network anodes produced here (1.85 V) are also higher than many other common anode materials, including PbO_2 (1.7 V), Pt (1.4 V), and IrO_2 (1.32 V), but are still lower than boron-doped diamond (BDD, 2.1 V).[28]

To further understand the oxygen-evolution kinetics, a Tafel analysis of the four electrodes was completed and is presented in Figure 2b. The Tafel plot, eq 5, describes the linear relationship between the anode potential E (mV) and the logarithm of the current I (A):[41]

$$E = a + b \log\{I\} \quad (5)$$

The slope b (V dec^{-1}) is known as the Tafel slope and is inversely related to the oxygen-evolution kinetics (i.e., a larger Tafel slope indicates slower oxygen-evolution kinetics). The unit, V dec^{-1} represents volts per decade of current. The Tafel slopes for the four materials follow the order uncoated CNT (black, 0.5 V dec^{-1}) < ATO-CNT (blue, 0.88 V dec^{-1}) < BTO-CNT (pink, 1.05 V dec^{-1}) < TO-CNT (red, 1.37 V dec^{-1}), in

agreement with the LSV data. The Tafel slopes of the TO-CNT and BTO-CNT are higher than many common anode materials including BDD (0.29 V dec^{-1}) and PbO_2 (0.18 V dec^{-1}),[42] indicating relatively slow oxygen-evolution kinetics. The LSV and Tafel analysis both indicate that the tin oxide and doped tin oxide nanoparticle coatings on the CNT networks can effectively increase the OEP and the Tafel slope relative to the uncoated CNT anode, resulting in both a delayed onset of water oxidation and slower oxygen-evolution kinetics (key challenge III).

Effect of Metal Oxide NP Coating on Organic Oxidation Performance. Although high-anode-material OEP usually indicates higher current and energy efficiency towards organic oxidation, rapid kinetics is also necessary for an effective electrooxidative processes. Thus, here, the recalcitrant organic oxalate was utilized as a target molecule for the initial oxidation experiments. Electrochemical anodic oxidation as well as other advanced oxidation processes (AOPs) have been previously studied for oxalate degradation[36,43−45] because it is the most common non-CO_2 end product during aromatic oxidation[36] as a result of its slow reaction with the $^{\bullet}OH$ radical ($C_2O_4^{2-} + {}^{\bullet}OH \rightarrow CO_2 + CO_2^{\bullet-}$; $k = 7.7 \times 10^6$ M^{-1} s^{-1}).[46] Oxalate and oxalic acid can undergo a two-electron oxidation process to carbonate/CO_2 according to the following equations:

$$C_2O_4^{2-} + 2OH^- \rightarrow 2CO_3^{2-} + 2H^+ + 2e^- \quad (E^o = 1.18\ V) \tag{6}$$

$$H_2C_2O_4 \rightarrow 2CO_2 + 2H^+ + 2e^- \quad (E^o = 0.345\ V) \tag{7}$$

The uncoated CNT, TO-CNT, ATO-CNT, and BTO-CNT were challenged by an aqueous oxalate solution (C_{in} = 100 mg L^{-1}, [Na_2SO_4] = 10 mM, J = 1.5 mL min^{-1}, and residence time 1.2 s). The TOC removal percentage and average total cell voltage of the uncoated CNT (black), TO-CNT (red), ATO-CNT (blue), and BTO-CNT (pink) as a function of the steady-state current (0−60 mA) are presented in Figure 3, panels a and b, respectively. The solid line (yellow) in Figure 3a is the theoretical maximum TOC removal, and the points are the experimental measurements. The TOC removal for the uncoated CNT anode first increases with increasing current to 62 ± 2.5% at 15 mA and then decreases significantly to only 26 ± 12.4% at 40 mA. A similar trend was observed for the TO-CNT anode, with TOC removal peaking at 40 mA (71 ± 4.4%) and then decreasing to 32 ± 23% when the current was increased to 60 mA. In contrast, the TOC removal for the ATO-CNT and BTO-CNT anodes increased until 89 ± 4 and 94 ± 4% TOC removal was achieved at ≥40 mA, respectively, and no TOC removal decrease with increasing current was observed. In regards to the maximum TOC removal rate over the current range of 0−60 mA, the ATO-CNT and BTO-CNT were 1.3 times greater than the TO-CNT because the Sb/Bi doping improved the conductivity and they were 1.5 times greater than the uncoated CNT anode because of a lesser oxygen evolution and improved anode stability, as will be discussed in detail later.

In Figure 3b, the total cell voltage of the electrochemical filter was observed to increase with increasing current for all four anode materials, and the voltage response was quite similar for all four anodes below 15 mA. For the uncoated CNT anode, the total cell voltage increased significantly at both 15 and 20 mA to 5.5 ± 0.5 V, which is the greatest among all of the materials, and reached 6.1 ± 1.9 V at 40 mA. The TO-CNT anode total cell voltage increased to values greater than the ATO and BTO at currents ≥40 mA, achieving 6.3 ± 1.7 V at 60 mA. In contrast, only a slight increase (slope 20−60 mA < slope 0−20 mA) in total cell voltage was observed for the ATO-CNT and BTO-CNT anodes when the current was >20 mA, reaching 4.7 ± 0.3 and 4.3 ± 0.2 V, respectively, at 60 mA.

The anodic TOC removal behavior in Figure 3a and the total cell voltage data in Figure 3b must be combined and compared with the anode electrochemical characterization results for a clear understanding of the material effect on anode efficacy and efficiency. At currents up to 10 mA, all four electrodes displayed similar performance: ∼50% TOC removal and >99% current efficiency near the theoretical maximum. The total cell voltage when I ≤10 mA was always <2.7 V, and this voltage results in an anode potential <1.1 V on the basis of previous CNT anode open-circuit potential measurements.[47] A 1.1 V anode potential is higher than the two-electron standard reduction potential of oxalate to carbonate (E^o = 0.98 V, pH 14; eq 6), but it is less than the OEP for all of the anode materials examined in this study (1.27−1.8 V vs Ag/AgCl), indicating the oxygen-evolution reaction is not active, which is in agreement with the similar oxidation performance of the four electrodes when I ≤10 mA. However, when the current was increased to ≥15 mA, the cell voltage for the uncoated CNT anode increased significantly to 4 V, indicating a dramatic decrease of anode conductivity with a corresponding decrease in TOC removal, as presented in Figure 3a. The increase of total cell voltage from 2.7 to 4 V will increase the anode potential to ∼2 V and over the OEP of the uncoated CNT, 1.27 V, activating oxygen evolution.

The passivation mechanism of the uncoated CNT anode at ≥4 V cell voltage may be attributed to two types of processes shown in Scheme 1: (a) electrochemical production of oxygen, eq 1, and subsequent formation of bubbles that can (a1) block reactive sites and (a2) mechanically break the CNT-CNT contacts and network and (b) CNT oxidative corrosion because of (b1) direct oxidation via the build-up of a high

Scheme 1. Representative CNT Passivation Mechanisms[a]

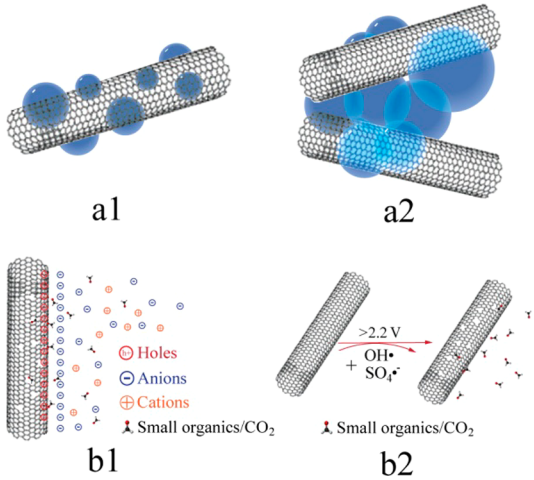

[a](a1)The produced oxygen bubbles block surface reactive electron transfer sites. (a2) The produced oxygen bubbles break CNT−CNT network contacts. (b1) Direct CNT oxidative corrosion resulting from surface hole accumulation, releasing small organics and CO_2. (b2) CNT oxidative corrosion resulting from hydroxyl radical and sulfate radical production at >2.2 V, releasing small organics and CO_2.

surface hole concentration and (b2) indirect oxidation via the production of homogeneous or surface-bound free radicals. In regards to mechanism a1, at potentials higher than the CNT OEP, significant oxygen evolution will produce a large amount of gas bubbles, which can be trapped in the porous CNT network and block the reactive surface for electrooxidation, leading to a decrease in the TOC removal rate. In regards to mechanism a2, at extended operation times, the bubbles will grow and expand in the porous network, resulting in the loss of CNT−CNT contact and the breakdown of network mechanical-stability, and both in turn will reduce network conductivity. The decrease of the uncoated CNT anode conductivity (i.e., significant increase in the total cell voltage with current) and TOC removal rate at ≥4 V cell voltage is likely due to mechanisms a1 and a2 because it coincides with the onset of the oxygen-evolution reaction. In regards to mechanisms b1 and b2, a high total cell voltage resulting from decreased network connectivity and conductivity will result in a high anode potential that will inevitably lead to CNT corrosion.[45] The CNT corrosion will decrease anode conductivity, resulting in a positive feedback that may rapidly aggravate anode passivation. Another consequence of CNT corrosion is the release of small organics into solution. CNT corrosion mechanisms b1 and b2 will be discussed in detail in the next section. In summary, the decrease in TOC removal by the uncoated CNT when I ≥15 mA is likely due to one of the previously discussed passivation mechanisms and is most likely a complex combination of the processes.

The TO-CNT displayed a better TOC removal rate than the uncoated CNT at ≥15 mA and had a similar TOC removal percentage as the ATO and BTO-CNT until I >40 mA. The increased stability of the TO-CNT as compared to the uncoated CNT is due to the high OEP and preferential hole transfer to the tin oxide coating, reducing passivation. However, a significant loss of electrochemical activity still occurred at 60 mA. The total cell voltage versus steady-state current did not display a sudden increase similar to the uncoated CNT, indicating bubble formation via oxygen evolution (mechanism a2) is not greatly affecting the conductivity because of the high OEP of TO-CNT. However, the cell voltage still increased up to 6.3 V and may have led to CNT corrosion and anode passivation. The higher total cell voltage of the TO-CNT at 60 mA as compared to ATO-CNT and BTO-CNT can be attributed to the semiconductive nature of the TO coating, which increases the overall electrical resistance of the anode network (i.e., SnO_2 is a semiconductor with a large band gap of 3.7 eV and limited conductivity if it is not doped).[28] For example, pure tin oxide has a low conductivity (0.01−1 Ω^{-1} cm^{-1}) that can be increased by doping with Sb (1−200 Ω^{-1} cm^{-1}) because of the creation of oxygen vacancies that increase the charge carrier concentration. For comparison, fabricated CNT yarns with a porosity of 75% have a conductivity of 200 Ω^{-1} cm^{-1}.[48−50] The low conductivity of SnO_2 indicates that at high steady-state currents the holes may preferentially flow through the more conductive CNTs, resulting in passivation. Therefore, as compared to the uncoated CNT and TO-CNT, the ATO-CNT and BTO-CNT benefited from both their high OEP and increased conductivity (e.g., at 40 mA, the ATO-CNT achieved an 89 ± 4% TOC removal with a cell voltage of 4.7 ± 0.4 V and the BTO-CNT achieved a 94 ± 4% TOC removal with a cell voltage of 4.3 ± 0.4 V without any indication of anode passivation).

The oxalate electrooxidation current efficiency as a function of the steady-state current for the CNT (black), TO-CNT (red), ATO-CNT (blue), and BTO-CNT (pink) anodes is displayed in Figure 3c (same experimental conditions as panels a and b). The bars represent the experimental measurements, and the solid line is the theoretical maximum current efficiency. The theoretical maximum current efficiency is calculated by setting TOC_{eff} = 0 in eq 3 and a maximum efficiency of 100%. All four anode materials had a current efficiency of >90% when I ≤10 mA, indicating minimal oxygen evolution, which is in agreement with the results presented in Figure 3a,b, and at higher steady-state currents (≥15 mA) the current efficiencies for all four anodes decreased relative to the theoretical maximum current efficiency. The oxalate oxidation current efficiency of the uncoated CNT anode decreased rapidly to 12.9% at 40 mA. Improvement was observed for the TO-CNT anode where the current efficiency was 34.3% at 40 mA, but it decreased to 10.3% at 60 mA. The ATO-CNT and BTO-CNT anodes had the highest oxalate oxidation current efficiency, which approached the theoretical maximum at all steady-state currents. At 40 mA, the current efficiency for the ATO-CNT and BTO-CNT anodes was 38.6 and 48.7%, respectively, which are more than 3 times greater than the uncoated CNT anode, 12.9%, and slightly less than the theoretical maximum CE of 60%. At 60 mA, the current efficiency of the ATO-CNT and BTO-CNT anodes was 30 and 32.2%, respectively, which again are more than 3 times the less conductive TO-CNT anode, 10.3%, and close to the theoretical maximum CE of 33%.

The energy consumption (kW h $kgTOC^{-1}$) for oxalate oxidation at the uncoated CNT (black), TO-CNT (red), ATO-CNT (blue), and BTO-CNT (pink) anodes are plotted in Figure 3d (same experimental conditions as a−c). All electrodes showed similar energy consumption (2.8−10.3 kW h $kgTOC^{-1}$) at currents ≤15 mA, but the ATO-CNT and BTO-CNT anodes had significantly lower energy consumption at higher steady-state currents. At 40 mA, the energy consumption of the ATO-CNT and BTO-CNT anodes are 24.4 and 17.1 kW h $kgTOC^{-1}$, respectively, which are 4 to 5 times less than the energy consumption of the uncoated CNT, 105.3 kW h $kgTOC^{-1}$. At 60 mA, the energy consumption of the ATO-CNT and BTO-CNT anodes were 35.2 and 30.4 kW h $kgTOC^{-1}$, respectively, which again are 4 to 5 times less than the energy consumption of the TO-CNT, 130.5 kW h $kgTOC^{-1}$. In practical applications, high current densities (>40 mA cm^{-2}) may be necessary to ensure rapid oxidation kinetics, and the ATO-CNT and BTO-CNT anodes significantly reduce (4 to 5 fold) the energy consumption under the highest current conditions utilized here by reducing competitive water oxidation. A comparison of oxalate oxidation kinetics and energy consumption by various anode materials and methods is presented in Table S1 along with detailed discussion in the Supporting Information.

Both ATO-CNT and BTO-CNT displayed similar efficacy and efficiency towards oxalate oxidation; however, antimony is a regulated toxic chemical. The EPA National Primary Drinking Water Regulations regulates a maximum contaminant level for antimony of 6 μg L^{-1},[33] whereas Bi is not regulated and can be found in common over the counters medicines such as Pepto-Bismol. Therefore, the BTO-CNT network was the most effective and efficient anode material because of the combination of high OEP, increased conductivity, and non-toxicity (key challenge III), and thus will be evaluated in greater detail relative to the uncoated CNT anode as a control.

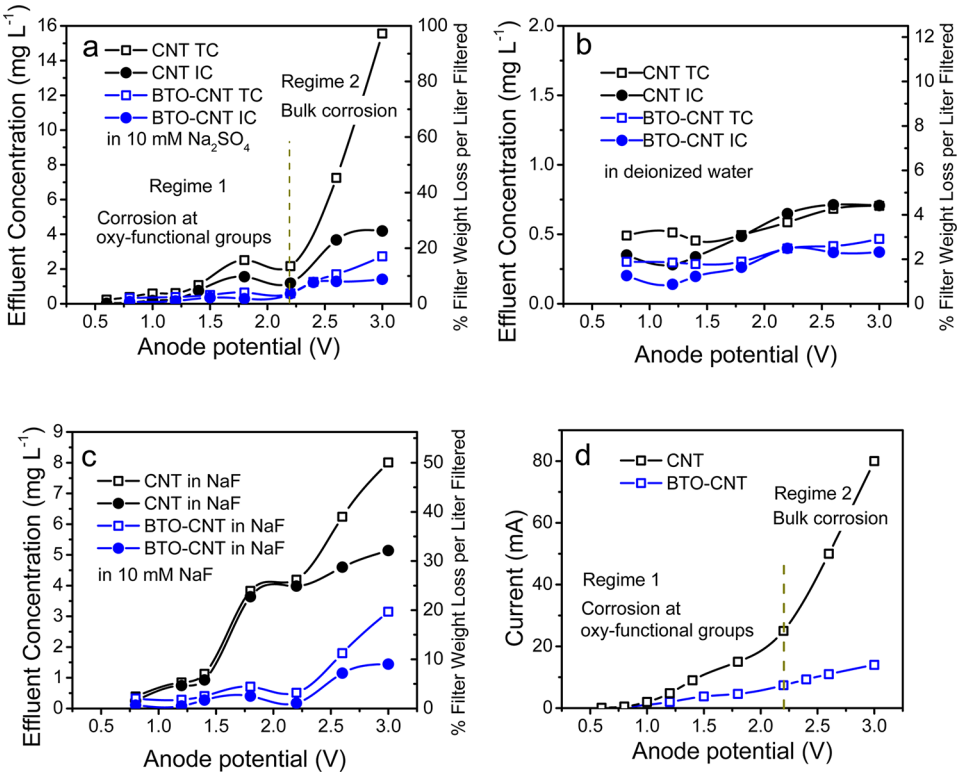

Figure 4. Anode stability test for the CNT and BTO-CNT anode. (a) Effluent total carbon (TC) (mg L^{-1}) and inorganic carbon (IC) (mg L^{-1}) at anode potentials ranging from 0.6 to 3.0 V for uncoated CNT (black) and BTO-CNT (blue) anodes in [Na_2SO_4] = 10 mM. Open squares are TC, and closed circles are IC. (b) Anode stability test in deionized water. (c) Anode stability test in 10 mM NaF. The flow rate, *J*, was 1.5 mL min^{-1}, and residence time was 1.2 s in all experiments. (d) Steady-state current at anode potentials ranging from 0.6 to 3.0 V for uncoated CNT (black) and BTO-CNT (blue) anodes. Regimes are labeled according to the dominating corrosion sites. Note the different *y*-axis scale for panels a–c.

Anode Stability Test. Anode corrosion stability is a critical factor in high-potential electrochemical applications. Many studies indicate that CNT anode corrosion will likely occur at increased anode potentials (>1.7 V for MWCNT and >1.0 V for SWCNT vs Ag/AgCl) in electrolyte solutions because of direct electrolyte-mediated oxidation (mechanism b1) or indirect free-radical oxidation (mechanism b2).[13,53,54] Anodic corrosion will decrease the CNT conductivity by damaging their sp^2 conjugation, leading to decreased current efficiencies and organic oxidation rates. It was reported that the resistivity of an SWCNT increased by over 4 orders of magnitude from ~120 to ~1.6×10^6 Ω sq^{-1} after being etched at an anode potential of 2.0 V.[54] To mineralize or even oxidize recalcitrant organics, high anode potentials are inevitable and thus the anode stability acts as an upper limit to the anode potential.

The anodic stability of the BTO-CNT and uncoated CNT network was evaluated by electrochemical filtration experiments with 10 mM Na_2SO_4, deionized water, and 10 mM NaF solutions (TC ≤0.1 mg L^{-1}), and the results are displayed in Figure 4a–c, respectively. The left vertical axis is the effluent TC and IC concentration in milligrams per liter, the right vertical axis is the percent anode mass loss per liter filtered, and the *x* axis is the anode potential (0.6–3.0 V). The percent anode mass loss per liter filtered was calculated by effluent TC (mg L^{-1}) divided the total weight of filter, 16 mg. The maximum filtration volume can then be calculated as the inverse of the percentage anode mass loss per liter filtered.

During the anode stability test, the TC and IC in the effluent should be minimal under potentials where the anode is stable because neither is in the influent. In the Na_2SO_4 experiments (Figure 4a), the uncoated CNT anode was stable (TC_{eff} < 0.6 mg L^{-1}) when V_{anode} <1.4 V and displayed two regimes of oxidative corrosion between 1.4–2.2 V and >2.2 V. Interestingly, between the anode potential range of 1.4–2.2 V, the uncoated CNT effluent TC (2.5 mg L^{-1}) and IC (1.6 mg L^{-1}) values peaked at 1.8 V, indicating a finite amount of electro-active reactant, such as the CNT surface functional groups, in agreement with previous literature where direct MWCNT etching was observed at >1.7 V.[54] At anode potentials ≥2.2 V, the effluent TC and IC increased rapidly to maxima of 15.6 and 4.2 mg L^{-1}, respectively, at 3.0 V. At this corrosion rate, it would take only 34 min to lose 5% of the CNT anode mass, and the maximum filtration volume would be only ~1 L before near complete anode corrosion.

The corrosion mechanism must be considered in two ways: the predominant corrosion sites and the predominant corrosion reaction. The oxidation peak at 1.8 V can be attributed to mostly direct electrooxidation of the CNT surface oxy-functional groups because of the high inorganic carbon (64%) and low organic carbon content of the effluent (e.g., surface carboxylates would be oxidized to CO_2 and surface carbonyls would be oxidized to CO). In contrast, at anode potentials ≥2.2 V, a high organic carbon (73%) and low inorganic carbon effluent content was observed and may be attributed to bulk corrosion of the CNTs via direct and indirect oxidation pathways.

From the perspective of the predominant corrosion reaction, the oxidative corrosion mechanisms proposed in Scheme 1, b1 and b2, the surface hole accumulation (>1.4 V), and the oxidative radicals production (>2.2 V), respectively, can explain

the anodic processes responsible for the TOC and IC production. In regards to mechanism b1, the electrolyte/semiconductor interface plays an important role in the anodic hole stabilization and the subsequent corrosion process[54] (i.e., under an anodic bias, the electrolyte forms a charged layer at the semiconductor surface that stabilizes interfacial charge carriers such as holes, resulting in anode corrosion) (Scheme 1, mechanism b1). In regards to mechanism b2, oxidative radicals produced from the water ($HO^{\bullet}$) and electrolyte ($SO_4^{\bullet-}$) oxidation may also contribute to CNT bulk corrosion at higher potentials (>2.2 V). At the neutral pH used in this study, anode potentials >2.2 V (vs Ag/AgCl), similar to the onset of the second oxidation regime, would be sufficient to produce hydroxyl radicals following eq 8.[51,52]

$$OH^- + h^+ \rightarrow OH^{\bullet} \quad (E^o = 2.1\ V,\ pH\ 7) \tag{8}$$

Similarly, at anode potentials >2.2 V (vs Ag/AgCl), the sulfate radical can be produced following eq 9:[52]

$$SO_4^{2-} + h^+ \rightarrow SO_4^{\bullet-} \quad (E^o = 2.2\ V) \tag{9}$$

Therefore, to test our hypothesis, stability tests for an uncoated CNT anode were completed in deionized water without electrolyte (only mechanism b2 via eq 8) and in an inert NaF electrolyte (only mechanisms b1 and b2 via eq 8). Fluoride is considered to be an oxidatively inert electrolyte at anode potentials <3 V because of its high standard reduction potential, eq 10:[52]

$$F^- + h^+ \rightarrow F^{\bullet} \quad (E^o = 3.4\ V) \tag{10}$$

During the stability test in deionized water (Figure 4b), the TC was equivalent to the IC, and both peaked at 3.0 V at 0.7 mg L^{-1} (~4% anode mass loss per liter filtered), indicating minimal corrosion in the absence of electrolyte. Only 4.4% of filter weight was lost per liter filtered at 3.0 V, and the maximum filtration volume would be 22.7 L before complete corrosion. Anodic water oxidation and hydroxyl radical production, eq 8, is also observed to be inactive and may be inhibited because of the high resistance of deionized water. The stability test in the inert electrolyte NaF in Figure 4c (in black) displayed a two oxidation regimes (1.5–2.2 and >2.2 V) similar to that of Na_2SO_4, and the peak TC concentration at 3 V was ~50% less (8 mg L^{-1}) than Na_2SO_4, indicating a strong contribution of sulfate oxidation, eq 9, to CNT corrosion at high potentials. Therefore, the no electrolyte/Na_2SO_4/NaF experiments indicate that CNT corrosion because of high surface hole concentration (Scheme 1; mechanism b1) is the dominant corrosion mechanism at 1.4 to 2.2 V because the TC/IC are similar in the sulfate and fluoride electrolytes but are negligible in the absence of electrolyte. At >2.2 V, free-radical production, eqs 8 and 9, (Scheme 1; mechanism b2) also contributes significantly to CNT oxidative corrosion (e.g., at 3 V sulfate contributes to ~50% of the corrosion)). Therefore, the maximum stable working potential for the uncoated CNT anode is 1.4 V and may be acceptable up to 2.2 V. The maximum filtration volume for the most extreme case (10 mM Na_2SO_4) of a 16 mg uncoated CNT anode was 15 L at 1.4 V and 7.4 L at 2.2 V.

In contrast, the BTO-CNT anode displayed significantly improved anode stability under all solution conditions (blue symbols in Figure 4a–c). For the 10 mM Na_2SO_4 electrolyte, the effluent TC and IC remained <0.6 mg L^{-1} up to anode potentials of 2.2 V, indicating minimal CNT corrosion at potentials necessary for the oxidation/mineralization of most species. The anode mass loss per liter filtered was only 3.75%, and the volumetric life span was increased to 26.7 L; 3-fold greater as compared to the uncoated CNT anode. The improved BTO-CNT anode stability at V_{anode} <2.2 V indicates that the BTO-NPs preferentially accumulate generated holes because they are at the outermost surface of the anode material and have a smaller radii of curvature (i.e., a higher local charge density, the tip effect).[55] A slight increase of effluent TC and IC for the BTO-CNT was observed between 2.2 and 3.0 V, but even at 3.0 V, the TC_{eff} = 2.7 mg L^{-1} and IC_{eff} = 1.4 mg L^{-1}. The anode mass loss per liter filtered was only 16.9%, and the volumetric life span was increased to 5.9 L, a 6-fold increase as compared to the uncoated CNT anode. The blue symbols in Figure 4b are the effluent TC and IC for the BTO-CNT corrosion in deionized water. Similar to the CNT stability test, the BTO-CNT corrosion in deionized water was minimal, with TC_{eff} <0.4 mg L^{-1} at V_{anode} = 3.0 V, indicating again that hole accumulation and radical formation (mechanisms b1 and b2) were inhibited in the absence of electrolyte. Similar to the uncoated CNT results, the BTO-CNT anode stability in 10 mM NaF (blue, Figure 4c) displayed two corrosion regimes at anode potentials from 1.4–2.2 and >2.2 V, with a maximum TC_{eff} = 3.1 mg L^{-1} at V_{anode} = 3 V. This TC_{eff} maximum was similar to that for Na_2SO_4, TC_{eff} = 2.7 mg L^{-1}, indicating that CNT oxidation by the sulfate radical did not contribute significantly to BTO-CNT corrosion. Thus, the BTO-CNT exhibited negligible corrosion up to 2.2 V (0.8 V higher than uncoated CNT anode) and significantly reduced corrosion up to 3.0 V.

The mass-normalized volumetric lifespan of the BTO-CNT anode is 2.6 m^3 $gCNT^{-1}$ when V_{anode} = 1.4 V and 1.7 m^3 $gCNT^{-1}$ when V_{anode} = 2.2 V. The energy consumption in this study for treating 1.7 m^3 water with $[Oxalate]_{in}$ = 100 mg C L^{-1} at a steady-state current of 40 mA was 3.06 kW h (a total electricity cost of $0.41 assuming an electricity price of $0.134 kW h^{-1}; US Energy Information Administration). The cost of 1 g of CNTs is <$0.1 and thus <25% of the energy costs.[56] Therefore, the major cost of high-potential water treatment using CNT-based anodes is the energetic operational costs. Nevertheless, the relatively short lifespan of the CNT-based anode is a drawback, and the development of CNT materials with greater anode stability should be a direction of future research.

The steady-state current, over a similar potential range of 0.4–3.0 V, is presented in Figure 4d. The uncoated CNT anode had a higher current than the BTO-CNT anode at V_{anode} >1 V, and the current difference increased with increasing potential. The higher uncoated CNT current is due to faster oxygen evolution (>1.27 V) and CNT corrosion kinetics (>1.4 V, mechanisms b1 and b2). The uncoated CNT anode current started to increase significantly at >1.2 V, around its OEP, and the current of the BTO-CNT started to increase at >2 V, again close to its OEP. Two regimes were labeled in Figure 4a,b according to the nature of the CNT sites that undergo oxidation, as previously discussed, with regime 1 (1.4–2.2 V) being predominantly mechanism b1 and regime 2, mechanisms b1 and b2 acting simultaneously. In regime 2 (V_{anode} >2.2 V), the max effluent TC was 15.6 mg C L^{-1} for the uncoated CNT anode, which is around 5.8-fold greater than the BTO-CNT at 2.7 mg C L^{-1}. Similarly, the max current for the uncoated CNT was ~80 mA, which is around 5.7-fold greater than the BTO-CNT anode at ~14 mA. In summary, the BTO-CNT exhibited

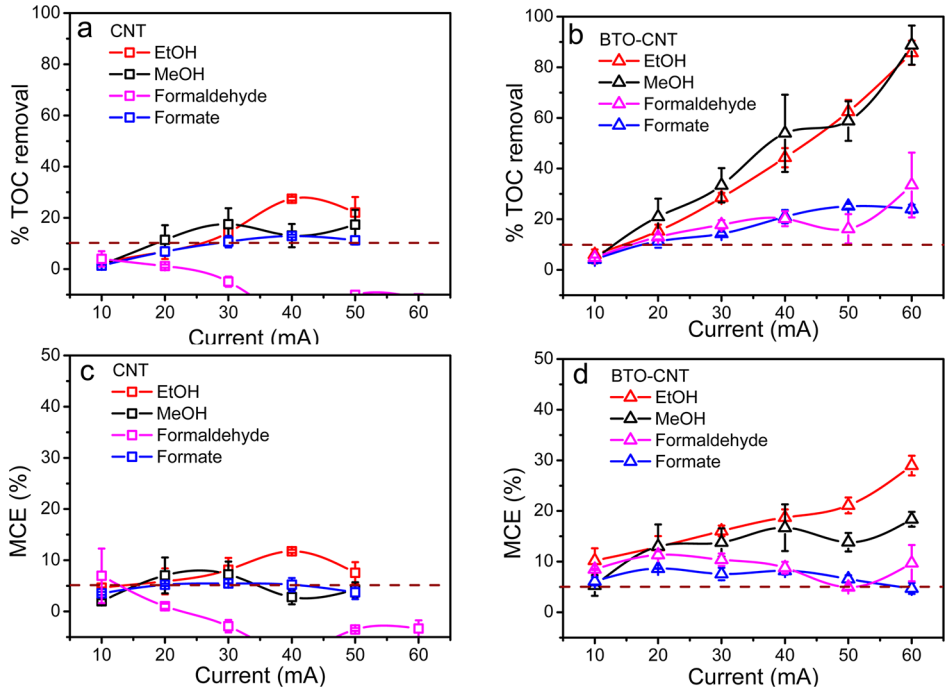

Figure 5. Electrooxidative filtration of various small dissolved organics. (a) TOC removal (%) on the CNT anode. (b) TOC removal (%) on the BTO-CNT anode. (c) Mineralization current efficiency (%) on the uncoated CNT anode. (d) Mineralization current efficiency (%) on the BTO-CNT anode. J = 3 mL min^{-1}, residence time 0.6 s, and influent TOC were [EtOH] = 7 mg C L^{-1}, [MeOH] = 5 mg C L^{-1}, [formaldehyde] = 11 mg C L^{-1}, [formate] = 20 mg C L^{-1}. [Na_2SO_4] = 10 mM was used as the background electrolyte.

significantly improved anode stability, extending the working potential upper limit to 2.2 V (800 mV higher than the CNT anode at 1.4 V) and increasing the anode lifetime by 6-fold at an anode potential of 3.0 V. The BTO-CNT anode also displayed a significantly lower water oxidation and corrosion current at all potentials.

To examine anodic CNT corrosion further, the surface elemental ratios of the uncoated CNT anode after oxidation at 1.8 V for 5 min and the BTO-CNT anode after oxidation at 3.0 V for 5 min were determined by XPS analysis and are listed in Table 1. For the oxidized and uncoated CNT anode, the surface was composed of 87.41% C, 9.82% O, 0.61% Fe, 1.57% Na, and 0.58% S by atomic ratio. The S and Na were attributed to residual electrolyte salt deposited on CNT network, and the Fe was the residual catalyst. Assuming that the O/S ratio in deposited salt is 4 and that the remainder is oxygen bound to carbon, the CNT surficial oxygen content is 7.5%. If we denote the oxygen bound to carbon as O−C, then the O−C/C ratio is 7.5%/87.41%, or 0.086. For comparison, the fresh CNTs have an O−C/C ratio of 0.005, indicating a significant amount of uncoated CNT anode surface oxidation. A similar O−C/C ratio calculation was carried out for the BTO-CNT anodes assuming the O/Sn ratio for tin oxide is 2, the O/Bi ratio for bismuth oxide is 1.5, and the O/S ratio for sulfate is 4. The estimation yields an O−C/C ratio of 0.023 for the fresh BTO-CNT and 0.034 for the BTO-CNT after the application of a 3.0 V anode potential for 10 min, indicating minor anode corrosion and oxidation as compared to the uncoated CNT. The improved stability against anodic corrosion/oxidation of BTO-CNT is a result of preferential hole accumulation in the SnO_2 nanoparticles reducing mechanism b1. The increased BTO-CNT OEP will also result in lesser water electrolysis, oxygen bubble formation, and oxidant production (mechanisms a1, a2, and b2). In summary, the XPS data supports the improved BTO-CNT anode stability (e.g., there is a minimal increase, 0.011, of CNT surface oxygen content increase with a BTO coating at 3 V in comparison to the increase, 0.081, observed for the uncoated CNT at 1.8 V).

General Organic Electrooxidative Filtration. The initial experiments have now shown the BTO-CNT anode to be a stable, environmentally friendly, and effective/efficient towards oxalate oxidation. To study the efficacy and efficiency of the BTO-CNT anode towards organic electrooxidation further, the anodic filter was challenged with a series of small organic molecules: ethanol, methanol, formaldehyde, and formate. Their selected physical/chemical properties are listed in Table S2 together with those of oxalate. Electrooxidation experiments were completed with [Na_2SO_4] = 10 mM, J = 3.0 mL min^{-1}, residence time = 0.6 s, and steady-state currents ranging from 10 to 60 mA. As a control, similar oxidation experiments were also conducted with an uncoated CNT anode. The influent concentrations for ethanol, methanol, formaldehyde, and formate were 7, 5, 11, and 20 mg C L^{-1}, respectively, such that they require a similar total number of electron transfers for mineralization. In the mineralization processes, ethanol and methanol require 6 e$^-$ transfers per carbon (3.5 and 2.5 mmol L^{-1}), formaldehyde, 4 e$^-$ per carbon (3.67 mmol L^{-1}), and formate, 2 e$^-$ per carbon (3.33 mmol L^{-1}). The effluent TOC was measured after the electrooxidation reached steady state (20 min) and was used to calculate the TOC removal percentage and mineralization current efficiency, as presented in Figure 5. For the uncoated CNT anode, the TOC removal of ethanol, methanol, and formate first increased with steady-state current because of faster reaction kinetics but then decreased because of the CNT anode passivation at high current/potential, in agreement with the oxalate results (Figures 3 and 4). The peak TOC removal by the uncoated CNT anode of ethanol, methanol, and formate are 27.5, 17.5, and 12.9%,

respectively. The formaldehyde TOC removal peaked at 4% (10 mA), decreased to 1% at 20 mA, and then became negative because the effluent TOC was greater than the influent TOC because of anode corrosion (Figure 4).

These experimental results yield insight into the anode passivation mechanisms during CNT electrochemical filtration and support the proposed mechanism in Scheme 1. The gradually decreasing TOC removal with increasing current for all four organic molecules studied here as well as oxalate provide evidence for oxygen evolution being a primary anode passivation mechanism. Oxygen evolution will not only compete with organic oxidation for current, eq 1, but will also produce oxygen bubbles that block reactive sites (Scheme 1; mechanism a1) and strain the CNT network structure, breaking the integrity and conductivity of the network (Scheme 1; mechanism a2). In addition, should oxygen evolution be the only passivation mechanism, the TOC in effluent should never exceed the influent TOC. However, the formaldehyde experiment displayed that the effluent TOC became greater than the influent TOC at over 20 mA (V_{anode} ~2 V, Figure 4d), clearly indicating that CNT corrosion is also an important passivation mechanism (Scheme 1; mechanisms b1 and b2).

The electrooxidation results of ethanol, methanol, formaldehyde, and formate by the BTO-CNT anode are presented in Figure 5b. In the ethanol and methanol electrooxidation experiments, a monotonic increase in TOC removal is observed with increasing steady-state current. At 60 mA, the BTO-CNT anode TOC removal was 85.7% (1.5×10^{-4} mg C s^{-1}) for ethanol and 88.7% (1.1×10^{-4} mg C s^{-1}) for methanol, a 3- and 5-fold increase in the mineralization rate, respectively, as compared to the uncoated CNT anode. The highest formaldehyde BTO-CNT TOC removal was 33.5% (0.92×10^{-4} mg C s^{-1}) at 60 mA, an 8-fold increase relative to the uncoated CNT anode. Formate electrooxidation by the BTO-CNT anode peaked at 25% removal (1.2×10^{-4} mg C s^{-1}) at both 50 and 60 mA, a 2-fold increase in the TOC removal relative to the uncoated CNT anode. In summary, the BTO-CNT anode displayed excellent TOC removal rate towards methanol, ethanol, and oxalate and improved TOC removal rates towards formaldehyde and formate, with a 2−8-fold increase in mineralization kinetics as compared to uncoated CNT anode. The origin of such performance may be attributed to three important factors: the conductivity of the BTO-CNT network, the high overpotential for and slow kinetics of oxygen evolution, and the improved anode stability towards CNT corrosion (key challenge III).

Some interesting findings were revealed by comparing the oxidation kinetics of oxalate, ethanol, methanol, formaldehyde, and formate on the BTO-CNT anode. Although all of the organic solutions have similar electron demands for mineralization, the TOC removal rates were quite different. Interestingly, oxalate, ethanol, and methanol had the highest TOC removal rate followed by formate and then formaldehyde, despite the fact that formate and formaldehyde have a smaller number of electrons per molecule for mineralization. The maximum electron transfer rates on the BTO-CNT anode were oxalate (2×10^{-7} mol s^{-1}) > ethanol (1.5×10^{-7} mol s^{-1}) > methanol (1.1×10^{-7} mol s^{-1}) > formaldehyde (6.2×10^{-8} mol s^{-1}) > formate (4.2×10^{-8} mol s^{-1}). In addition, the maximum TOC removal rates on the BTO-CNT anode were oxalate (2.4×10^{-3} mg C s^{-1}) > ethanol (3×10^{-4} mg C s^{-1}) > formate (2.4×10^{-4} mg C s^{-1}) > methanol (2.2×10^{-4} mg C s^{-1}) > formaldehyde (1.8×10^{-4} mg C s^{-1}), respectively. The significantly higher TOC removal rate of oxalate oxidation indicates that oxalate strongly sorbs to the anode surface, which would increase effective filter residence time and reduce the barrier to direct electron transfer. The similar electron transfer rates of methanol and ethanol to oxalate suggest that they also sorb well to the tin oxide surface. Similar to our observation, Stucki reported that the oxidation rate and current efficiency of ethanol was higher than formic acid on an ATO anode.[57] This result indicates the formaldehyde and formate molecules are not intermediates during mineralization of methanol (i.e., methanol is oxidized through a multi-electron transfer mechanism directly to CO_2 on the BTO-CNT anode).

To understand the predominant oxidation pathways further, kinetic calculations of the pseudo-first-order rate coefficient observed (k_{obs}) at different currents (10−60 mA) for the four organics were completed and then normalized with respect to the ethanol oxidation rate coefficient, $k^0_{obs} = k_{obs}/k^{EtOH}_{obs}$. At each current, the k^0_{obs} values of the organics are compared with normalized bimolecular reaction rate constants (with respect to ethanol) of $OH^\bullet$ ($k^0_{OH\bullet+S} = k_{OH\bullet+S}/k^{EtOH}_{OH\bullet+S}$) and $SO_4^{\bullet-}$ ($k^0_{SO_4\bullet^-+S} = k_{SO_4\bullet^-+S}/k^{EtOH}_{SO_4\bullet^-+S}$). The detailed calculation steps can be found in the Supporting Information. The kinetic rate coefficients are listed in Table S3, and the relationships of k^0_{obs} versus $k^0_{OH\bullet+S}$ and k^0_{obs} versus $k^0_{SO_4\bullet^-+S}$ are plotted in Figure S5. There is neither a correlation between k^0_{obs} and $k^0_{OH\bullet+S}$ data nor a correlation between k^0_{obs} and $k^0_{SO_4\bullet^-+S}$. This indicates that direct organic oxidation on the anode surface is the dominating oxidation pathway in the electrochemical filtration system examined here and supports the conclusion that stronger organic−metal oxide sorption results in faster and more effective mineralization kinetics.

The mineralization current efficiency (MCE) for organic oxidation on the CNT and BTO-CNT anodes are presented in Figure 5, panels c and d, respectively. Similar trends to the TOC removal results are observed for both the CNT and BTO-CNT anodes as discussed in the Supporting Information. Overall, the BTO NP coating on the CNT improved the MCE of anode by 50 to 1100% in the organic electrooxidation experiments. Of note is that the TOC removal and MCE increase rapidly with increasing current for alcohols but not as rapidly for formate and formaldehyde on the BTO-CNT anode, indicating that another process other than electron or mass transfer is mediating the overall oxidation kinetics. A previous study demonstrated a three step reactive transport mechanism during CNT electrochemical filter organic electrooxidation consisting of (1) mass transport, (2) sorption, and (3) electron transfer.[9] Should electron transfer be the only rate limiting step in the direct anodic oxidation of organics, then the responses of TOC removal and MCE to current should exhibit similar percentage increases for all four organics. Mass transport is also often an important step in electrooxidation processes, but it cannot be the cause of the significant differences observed here because all of the target molecules have a similar molecular weight and thus diffusion coefficient and are convectively transported at the same experimental flow rate of 3.0 mL min^{-1}. Thus, the different TOC removal and MCE of alcohols, formaldehyde, formate, and oxalate is likely due to their different sorption kinetics onto electrode surface.

CONCLUSIONS

A binder-free, conductive, and stable CNT 3D porous network with a BTO nanoparticle coating was successfully prepared via a sequential electrosorption−hydrothermal method in this study. The high oxygen-evolution potential (1.71 V), improved conductivity, and high porosity of the BTO-CNT network make it a promising anode material for electrooxidative filtration. The BTO coating has a thickness of <10 nm and is composed of nanoparticles of 3.9 ± 1.5 nm in diameter. The surface Bi/Sn atomic ratio is 0.02, as determined by XPS analysis. The BTO-CNT anode displayed the fastest oxalate electrooxidation kinetics, with up to 98% TOC removal of 100 mg C L^{-1} in a single pass of 1.2 s residence time (3×10^{-8} mol s^{-1} cm^{-2}), which is ∼32% faster than the TO-CNT because of Bi doping and ∼53% faster than the uncoated CNT anode. The current efficiency of BTO-CNT was over 3-fold higher and consumed 5-fold less energy than the uncoated CNT at a current supply of 40 mA. The energy consumption of the BTO-CNT anode was 25.7 kW h $kgCOD^{-1}$ at 40 mA with 90% TOC removal, comparable to state-of-the-art electrochemical oxidation (average range of 5−100 kW h $kgCOD^{-1}$) and near the lower end of energy consumption reported for oxalate oxidation (22.5−81.7 kW h $kgCOD^{-1}$). A comparison (uncoated CNT vs BTO-CNT) of the steady-state-current-dependent TOC and CE values for oxalate electrooxidation combined with the anode stability data yielded information on the CNT passivation mechanisms at high steady-state currents. Anode passivation is observed to be due to electrochemical water oxidation, eq 1, yielding oxygen bubbles that can (a1) block reactive sites and (a2) mechanically break the CNT network connectivity and conductivity as well as CNT corrosion resulting from (b1) direct CNT oxidation because of increased surface hole concentration and (b2) indirect oxidation via free-radical production. In regards to the corrosion sites, the surface oxy-functional groups oxidation was predominant between 1.4−2.2 V, and rapid CNT bulk corrosion occurs at >2.2 V. In regards to the corrosion reactions, direct corrosion because of electrolyte-stabilized high surface holes concentration is the dominant mechanism at ≥1.4 V (mechanism b1), and free-radical production from water and sulfate oxidation also contributes at ≥2.2 V (mechanisms b1 and b2). The redox stability of the BTO-CNT anode against corrosion was observed up to 2.2 V, which is >800 mV higher than the uncoated CNT anode. In agreement with the proposed mechanism, the significantly improved TOC removal, CE, and stability of the BTO-CNT anode relative to the CNT anode can be attributed to a high OEP resulting in less oxygen evolution and reduced exposure to surface holes. The maximum filtration volume of BTO-CNT was estimated to be 2.6 m^3 $gCNT^{-1}$ at 1.4 V and 1.7 m^3 $gCNT^{-1}$ at 2.2 V. The electrooxidative filtration experiments of four types of organic molecules, ethanol, methanol, formaldehyde, and formate, showed that the BTO-CNT anode achieved a significantly higher (2−8-fold) TOC removal and (0.5−11-fold) MCE than the uncoated CNT anode. The BTO-CNT nanocomposite porous electrode has promise for high-potential anode applications, and subsequent research should be on novel composites to extend the anode lifetime further.

ASSOCIATED CONTENT

Supporting Information

Pseudo-first-order rate coefficient calculation for small organics, images of the electrochemical filtration set up, XPS survey scans of four anode materials, mass percentage as a function of temperature for CNT and BTO-CNT in TGA, and relationships of k^0_{obs} versus $k^0_{OH\bullet+S}$ and k^0_{obs} versus $k^0_{SO_4\bullet^-+S}$. This material is available free of charge via the Internet at http://pubs.acs.org.

AUTHOR INFORMATION

Corresponding Author

*E-mail: vecitis@seas.harvard.edu; Phone: (617) 496-1458.

Notes

The authors declare no competing financial interest.

ACKNOWLEDGMENTS

We thank Harvard's Center for Nanoscale Systems (CNS) for SEM, TEM, and XPS. We thank Harvard's Material Research Science and Engineering Center (MRSEC) for TGA.

REFERENCES

(1) Xue, L. G.; Xu, G. J.; Li, Y.; Li, S. L.; Fu, K.; Shi, Q.; Zhang, X. W. *ACS Appl. Mater. Interfaces* **2013**, *5*, 21−25.
(2) Lee, S. W.; Yabuuchi, N.; Gallant, B. M.; Chen, S.; Kim, B. S.; Hammond, P. T.; Shao-Horn, Y. *Nat. Nanotechnol.* **2010**, *5*, 531−537.
(3) Sharma, R. K.; Zhai, L. *Electrochim. Acta* **2009**, *54*, 7148−7155.
(4) Rosario-Canales, M. R.; Deria, P.; Therien, M. J.; Santiago-Aviles, J. J. *ACS Appl. Mater. Interfaces* **2012**, *4*, 102−109.
(5) Guo, D. J. *J. Power Sources* **2011**, *196*, 679−682.
(6) Aravind, S. S. J.; Ramaprabhu, S. *ACS Appl. Mater. Interfaces* **2012**, *4*, 3805−3810.
(7) Vecitis, C. D.; Gao, G. D.; Liu, H. *J. Phys. Chem. C* **2011**, *115*, 3621−3629.
(8) Yang, J.; Wang, J.; Jia, J. P. *Environ. Sci. Technol.* **2009**, *43*, 3796−3802.
(9) Liu, H.; Vecitis, C. D. *J. Phys. Chem. C* **2012**, *116*, 374−383.
(10) Gao, G. D.; Vecitis, C. D. *ACS Appl. Mater. Interfaces* **2012**, *4*, 1478−1489.
(11) Wang, H. J.; Yin, G. P.; Shao, Y. Y.; Wang, Z. B.; Gao, Y. Z. *J. Power Sources* **2008**, *176*, 128−131.
(12) Zhuo, Q. F.; Deng, S. B.; Yang, B.; Huang, J.; Yu, G. *Environ. Sci. Technol.* **2011**, *45*, 2973−2979.
(13) Ohmori, S.; Saito, T. *Carbon* **2012**, *50*, 4932−4938.
(14) Li, W. Z.; Liang, C. H.; Zhou, W. J.; Qiu, J. S.; Zhou, Z. H.; Sun, G. Q.; Xin, Q. *J. Phys. Chem. B* **2003**, *107*, 6292−6299.
(15) Mu, Y. Y.; Liang, H. P.; Hu, J. S.; Jiang, L.; Wan, L. J. *J. Phys. Chem. B* **2005**, *109*, 22212−22216.
(16) Wang, N.; Wu, C. X.; Li, J. X.; Dong, G. F.; Guan, L. H. *ACS Appl. Mater. Interfaces* **2011**, *3*, 4185−4189.
(17) Honda, K.; Yoshimura, M.; Kawakita, K.; Fujishima, A.; Sakamoto, Y.; Yasui, K.; Nishio, N.; Masuda, H. *J. Electrochem. Soc.* **2004**, *151*, A532−A541.
(18) Liu, X. M.; Huang, Z. D.; Oh, S.; Ma, P. C.; Chan, P. C. H.; Vedam, G. K.; Kang, K.; Kim, J. K. *J. Power Sources* **2010**, *195*, 4290−4296.
(19) Shen, L. F.; Yuan, C. Z.; Luo, H. J.; Zhang, X. G.; Xu, K.; Zhang, F. *J. Mater. Chem.* **2011**, *21*, 761−767.
(20) Georgakilas, V.; Kordatos, K.; Prato, M.; Guldi, D. M.; Holzinger, M.; Hirsch, A. *J. Am. Chem. Soc.* **2002**, *124*, 760−761.
(21) Eder, D. *Chem. Rev.* **2010**, *110*, 1348−1385.
(22) Zhai, C. X.; Du, N.; Zhang, H.; Yu, J. X.; Yang, D. R. *ACS Appl. Mater. Interfaces* **2011**, *3*, 4067−4074.
(23) Besteman, K.; Lee, J. O.; Wiertz, F. G. M.; Heering, H. A.; Dekker, C. *Nano Lett.* **2003**, *3*, 727−730.

(24) Muguruma, H.; Hoshino, T.; Matsui, Y. *ACS Appl. Mater. Interfaces* **2011**, *3*, 2445−2450.
(25) Wu, Y.; Wei, Y.; Wang, J. P.; Jiang, K. L.; Fan, S. S. *Nano Lett.* **2013**, *13*, 818−823.
(26) Reddy, A. L. M.; Shaijumon, M. M.; Gowda, S. R.; Ajayan, P. M. *Nano Lett.* **2009**, *9*, 1002−1006.
(27) Wen, Z.; Wang, Q.; Zhang, Q.; Li, J. *Adv. Funct. Mater.* **2007**, *17*, 2772−2778.
(28) Panizza, M.; Cerisola, G. *Chem. Rev.* **2009**, *109*, 6541−6569.
(29) Zhao, G. H.; Cui, X.; Liu, M. C.; Li, P. Q.; Zhang, Y. G.; Cao, T. C.; Li, H. X.; Lei, Y. Z.; Liu, L.; Li, D. M. *Environ. Sci. Technol.* **2009**, *43*, 1480−1486.
(30) Han, W. Q.; Zettl, A. *Nano Lett.* **2003**, *3*, 681−683.
(31) Ren, J.; Yang, J.; Abouimrane, A.; Wang, D.; Amine, K. *J. Power Sources* **2011**, *196*, 8701−8705.
(32) Kim, J.C.; Hwang, I.S.; Seo, S.D.; Lee, G.H.; Shim, H.W.; Park, K.S.; Kim, D.W. *Nanotechnology* **2012**, *23*, 465402.
(33) USEPA National Primary Drinking Water Regulations Home Page. http://water.epa.gov/drink/contaminants/index.cfm.
(34) Chen, F. T.; Yu, S. C.; Dong, X. P.; Zhang, S. S. *J. Hazard. Mater.* **2012**, *227*, 474−479.
(35) Lee, K.S.; Park, I.S.; Cho, Y.H.; Jung, D.S.; Jung, N.; Park, H. Y.; Sung, Y. E. *J. Catal.* **2008**, *258*, 143−152.
(36) Garcia-Segura, S.; Brillas, E. *Water Res.* **2011**, *45*, 2975−2984.
(37) Zhang, H. X.; Feng, C.; Zhai, Y. C.; Jiang, K. L.; Li, Q. Q.; Fan, S. S. *Adv. Mater.* **2009**, *21*, 2299−2304.
(38) Slater, J. C. *J. Chem. Phys.* **1964**, *41*, 3199−3204.
(39) Li, X. Y.; Cui, Y. H.; Feng, Y. J.; Xie, Z. M.; Gu, J. D. *Water Res.* **2005**, *39*, 1972−1981.
(40) Zhu, J. J.; Lu, Z. H.; Aruna, S. T.; Aurbach, D.; Gedanken, A. *Chem. Mater.* **2000**, *12*, 2557−2566.
(41) Bard, A. J. *Electrochemical Methods: Fundamentals and Application*, 2nd ed.; John Wiley & Sons, Inc.: New York, 2001; pp 92−105.
(42) Zhao, G. H.; Zhang, Y. G.; Lei, Y. Z.; Lv, B. Y.; Gao, J. X.; Zhang, Y. A.; Li, D. M. *Environ. Sci. Technol.* **2010**, *44*, 1754−1759.
(43) Onder, E.; Koparal, A. S.; Ogutveren, U. B. *Chem. Eng. J.* **2009**, *147*, 122−129.
(44) Martinez-Huitle, C. A.; Ferro, S.; Reyna, S.; Cerro-Lopez, M.; De Battisti, A.; Quiroz, M. A. *J. Braz. Chem. Soc.* **2008**, *19*, 150−156.
(45) Huang, Y. H.; Shih, Y. J.; Liu, C. H. *J. Hazard. Mater.* **2011**, *188*, 188−192.
(46) Vecitis, C. D.; Lesko, T.; Colussi, A. J.; Hoffmann, M. R. *J. Phys. Chem. A* **2010**, *114*, 4968−4980.
(47) Gao, G.; Vecitis, C. D. *Environ. Sci. Technol.* **2011**, *45*, 9726−9734.
(48) Bansal, S.; Pandya, D. K.; Kashyap, S. C. *Thin Solid Films* **2012**, *524*, 30−34.
(49) Miao, M. *Carbon* **2011**, *49*, 3755−3761.
(50) Stjerna, B.; Olsson, E.; Granqvist, C. G. *J. Appl. Phys.* **1994**, *76*, 3797−3817.
(51) Bratsch, S. G. *J. Phys. Chem. Ref. Data* **1989**, *18*, 1−21.
(52) Wardman, P. *J. Phys. Chem. Ref. Data* **1989**, *18*, 1637−1755.
(53) Liu, C. M.; Cao, H. B.; Li, Y. P.; Xu, H. B.; Zhang, Y. *Carbon* **2006**, *44*, 2919−2924.
(54) Wei, D.; Liu, Y.; Cao, L.; Zhang, H.; Huang, L.; Yu, G.; Kajiura, H.; Li, Y. *Adv. Funct. Mater.* **2009**, *19*, 3618−3624.
(55) Enze, L. *J. Phys. D: Appl. Phys.* **1986**, *19*, 1−6.
(56) De Volder, M. F. L.; Tawfick, S. H.; Baughman, R. H.; Hart, A. J. *Science* **2013**, *339*, 535−539.
(57) Stucki, S.; Kotz, R.; Carcer, B.; Suter, W. *J. Appl. Electrochem.* **1991**, *21*, 99−104.